International Journal of Thermophysics, Vol. 20, No. 4, 1999

Measurement of the Electrical Conductivity of Metals in the Vicinity of the Critical Point[1]

A. W. DeSilva[2, 3] and J. D. Katsouros[2]

Measurement of the electrical conductivity of metal plasmas at near-solid densities is made possible by rapid vaporization of metal wires in water. The water acts as a tamper, slowing the expansion of the plasma and ensuring a well-defined cylindrical boundary. Measurement of the time-varying resistance is straightforward, and the conductivity and density are easily deduced after the column diameter is measured photographically. Temperature may be deduced from the measured energy input with help of an equation of state provided by the LANL SESAME tables. Measurements have been made on copper, aluminum, and tungsten plasmas. The electrical conductivity is almost independent of temperature at the highest densities. Conductivity falls steeply with falling density and reaches a minimum at a few percent of solid density, rising with further reduction in density. Near the minimum, the temperature dependence of the conductivity becomes appreciable.

KEY WORDS: electrical resistivity; pulse heating; strongly coupled plasma; copper; aluminum; tungsten.

1. INTRODUCTION

We have utilized the technique of rapid vaporization of wire by an electrical current to create dense, strongly coupled metal plasmas for which independent and accurate measurements of the mass density and electrical conductivity may be made over a wide range of densities We deduce the plasma temperature with the aid of the SESAME equation of state tables generated by the Los Alamos National Laboratory. In previously reported

[1] Paper presented at the Fifth International Workshop on Subsecond Thermophysics, June 16–19, 1998, Aix en Provence, France.

[2] Institute for Plasma Research, University of Maryland, College Park, Maryland 20742, U.S.A.

[3] To whom correspondence should be addressed.

0195-928X/99/0700-1267$16.00/0

work, we have presented measurements on copper and aluminum plasmas in the temperature range of 10,000 to 30,000 K [1, 2]. Here we report some results at lower temperatures, and include measurements in tungsten plasmas.

Exploding wire plasmas have been widely studied, and strongly coupled plasmas are produced in these discharges. However, in the case of unconfined wire explosions, the density of the resulting plasma is ill-defined, making precise measurement of the properties of the dense plasma difficult. In addition, instabilities tend to produce axially nonuniform plasmas, making interpretation of conductivity measurements uncertain [3].

Strongly coupled plasmas created by high current discharges in alkali metals and noble gases in capillaries have been studied [4–6] for plasma densities in the range of $10^{20}\,\mathrm{cm}^{-3}$, and a measurement of the electrical conductivity of the plasma resulting from evaporating material from the inner wall of a capillary in polyethylene has been reported [7].

2. EXPERIMENTAL METHOD

The metal under study, a wire, typically 0.125 to 0.250 mm in diameter and 26 mm long, is stretched between two electrodes immersed in a water bath (Fig. 1). A capacitor bank having a capacity of 3.86 μF is connected via a low-inductance path to one of the electrodes. Current is switched by a pressurized sparkgap switch. The inductance of the circuit, exclusive of the wire load, is about 230 nH. Additional inductance or series resistance may be inserted between the capacitor and the switch, giving a degree of control over the current waveform. A Rogowski belt surrounds the main electrode to measure the time derivative of the current, and a resistive voltage divider is used to measure the voltage at the load.

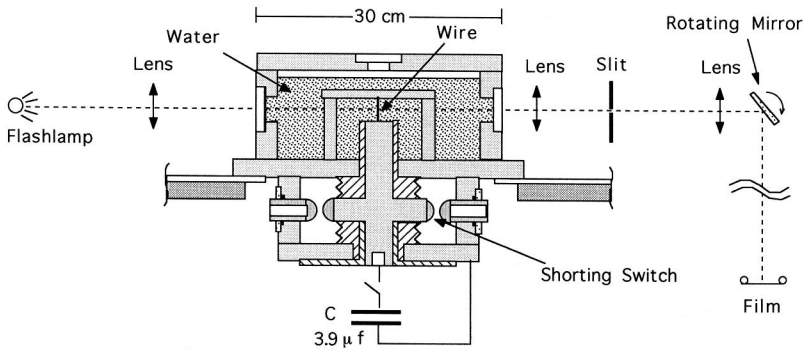

Fig. 1. Schematic of the experiment. The chamber is a cylinder with the wire on the axis.

Circuit parameters may be measured by installing a cylindrical plug in place of the wire load, and firing. Such a load is essentially purely inductive, and it is from the observed ringing period that the circuit inductance is determined. The voltage and current may be recorded for this inductive load, and subsequent comparison of $V(t)$ with $dI(t)/dt$ serves to confirm that the diagnostics are functioning correctly, and from the ratio of these quantities, the overall circuit inductance may be determined.

Light from the plasma is focused on a slit oriented perpendicular to the wire, which passes this image to a rotating mirror streak camera that records the time history of the plasma column diameter at 2.67:1 magnification. A xenon flashlamp is used to backlight the wire, making the plasma column visible in silhouette. A shock wave propagating through the water is clearly visible, since the density gradient at the shockfront strongly refracts the backlight. The plasma itself is opaque to the backlight and is also easily seen. The plasma diameter is easily measurable, and assuming validity of the assumption of uniform plasma density within the column, the density may then be deduced.

3. DATA ANALYSIS

Full vaporization of the wire occurs in a few hundred nanoseconds, during the rising phase of the current, at which time the rapidly rising resistance of the wire causes the current to decrease and the voltage across the plasma to increase. This voltage has both ohmic and reactive components and may be represented by

$$V = IR + LdI/dt + IdL/dt \tag{1}$$

where I is the current, L is the inductance of the current channel, and R is the ohmic resistance of the channel. In order to measure the plasma conductivity, we need the ohmic resistance R. L has been measured as described in Section 2, and its magnitude changes only slightly as the plasma column expands, so the term arising from IdL/dt may be neglected. We record the voltage and both the current and its derivative, and solve the above equation to find R.

Pressures generated in the expanding plasma range up to 50 kbar and rise to a maximum in less than 0.5 μs. The plasma expansion drives a shock wave in the surrounding water, and the high pressure behind the shock serves to inhibit the plasma column expansion. An estimate of thermal energy transfer between plasma and water indicates that the thickness of the plasma–water transition layer grows to only a few microns on the time scale of the experiment. We assume in the analysis that the wire vaporizes

fully and that the plasma fills the column uniformly, so a measurement of diameter of the column from the streak photograph allows us to calculate the plasma density throughout the expansion. Knowing the resistance and the column diameter, it is simple to compute the conductivity. A single shot therefore yields a record of the conductivity over a wide range of density, albeit at varying temperatures.

A pyrometric measurement of temperature would yield only the surface temperature in the water–plasma interface region and would not represent the true plasma temperture. Since such a direct measurement of temperature is not possible, we use an indirect method that depends on the SESAME equation of state database developed by the Los Alamos National Laboratory. This database gives pressure and internal energy of the metal on a grid of density versus temperature. In the case of the SESAME tables for copper, several theoretical models are used to describe different regions of the temperature–density parameter space, with interpolation between non-overlapping regions [8].

As the plasma expands, compression of the surrounding water and the resulting shock wave in the water may be described with a one-dimensional cylindrical Lagrangian code due to Plooster [9]. This code models the water as a series of 60 nesting cylindrical mass shells and uses the equation of state for water given by Rice and Walsh [10].

We record the current and voltage at 5-ns intervals, which is the natural time step for analysis. In each time step, we first compute the energy input to the plasma, using the measured voltage and current, and then consult the SESAME tables to find the pressure change at constant density. This new pressure is then inserted into the Lagrangian code to advance the motion of the water–plasma interface by one time step, resulting in a new plasma diameter and, hence, a new density. The SESAME data are then used again to find the new temperature and pressure, with the plasma expansion now treated as adiabatic. This process is repeated for as many time steps as have been recorded (typically 1000 at 5 ns per time step, followed by 700 at 20 ns per time step). The longer time step used in latter times is allowed since the plasma is changing at a slower rate.

Figure 2 displays the time record of a typical discharge made using a copper wire 0.25 mm in diameter. The top two traces show the recorded voltage, corrected by subtraction of the reactive component, and the current, electronically recorded using an RC integrator. (The current may also be found from numerical integration of the recorded dI/dt trace, but no significant difference is seen between the results of the two methods.) The mass density of the plasma may be deduced from measurements of the column diameter from the streak photographs. The rest of the curves, giving the density, pressure, temperature, and conductivity, are deduced

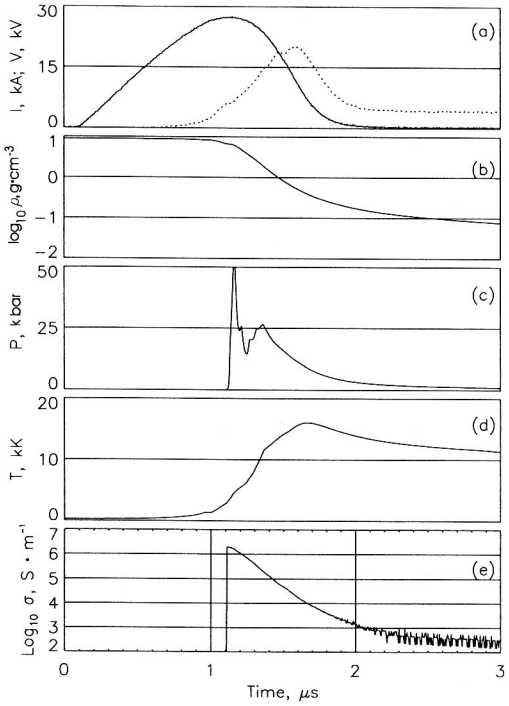

Fig. 2. Time history of a shot with a 0.25-mm-diameter copper wire at 12 kV initially on the capacitor. (a) Current (solid line) and voltage (dashed line). (b) Mass density. (c) Pressure. (d) Temperature. (e) Electrical conductivity. The electrical conductivity is calculated only for times after the temperature reaches the vaporization temperature.

from these data in the manner described above. Conductivity is determined from the relation

$$\sigma = \frac{1}{\pi r^2 R}$$

where σ represents the conductivity, R the column resistance, and r the column radius.

Comparison of the plasma expansion as calculated numerically with the plasma diameter measured from the streak photo shows close agreement (Fig. 3), lending confidence to the use of the numerical model to find the temperature.

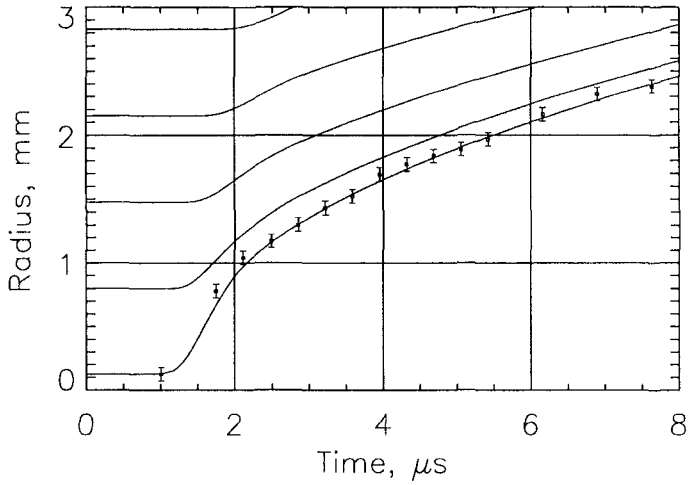

Fig. 3. Comparison of the plasma radius measured from a streak photo with results of numerical analysis using the SESAME data. Solid lines show the first five grid radii from the Lagrangian code. The lower line represents the plasma–water boundary. Points are measured radii from the streak photo.

At the early stage when the temperature is below the melting temperature, energy input to the wire is computed from I^2Rdt, using the measured current and published data for the wire resistance, and the heating is computed using published data for the specific heat. In this stage, the voltage across the wire is dominated by the reactive contribution, and relatively large errors result from use of a resistance calculated using Eq. (1). By the time the wire begins to vaporize, the ohmic voltage has risen considerably, and from this point on, the energy input is computed from $VIdt$.

In order to make clear the conditions through which the vapor/plasma passes, we display in Fig. 4a the pressure–volume relation at several temperatures from the SESAME database for copper, on which we have superposed the trajectory of a typical single shot. The left end of the trace starts when vaporization of the wire begins, and we see a rise in pressure and temperature, followed by an expansion and decay of temperature and pressure. Figures 4b and c show similar plots for aluminum and tungsten.

Analysis of a large number of discharges, with varying charge voltages and external resistances, allows us to find the conductivity at a variety of temperatures and densities. From individual shot profiles we select data at computed temperatures that lie within a narrow range (± 3 to 5%) around a selected temperature and plot the conductivity for these "target" temperatures versus density. Results are shown for copper in Fig. 5 and for

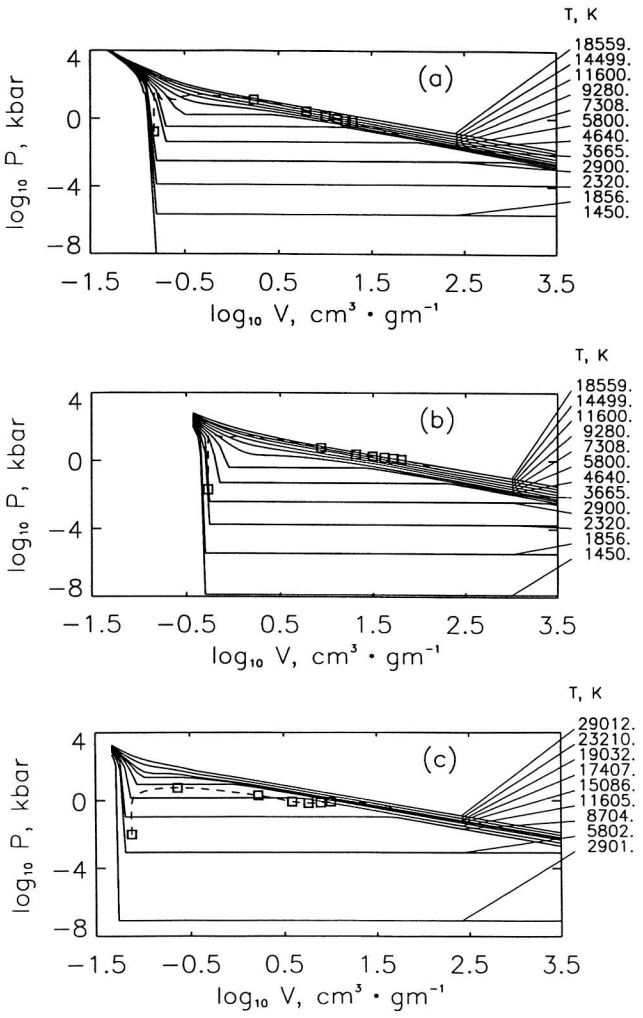

Fig. 4. Isotherms in the P–V plane from the SESAME database for (a) copper, (b) aluminum, and (c) tungsten. The path followed by a typical single shot is shown on each as a dashed line. Squares on the line indicate 0.5-μs intervals, counting from the time vaporization begins.

tungsten in Fig. 6. The tungsten data are given for a higher set of temperatures, corresponding to the higher temperatures at which the tungsten phase transitions occur. Typically, the conductivity falls rapidly with falling density, reaches a minimum, and then rises, eventually at the lowest densities approaching the Spitzer conductivity appropriate for dilute plasmas.

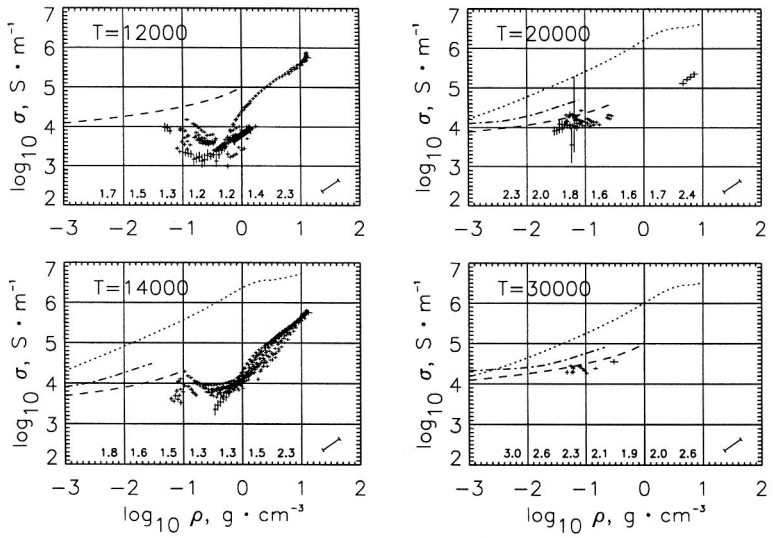

Fig. 5. Electrical conductivity of copper versus density at four temperatures spanning the critical temperature. Error bars represent uncertainties due to digital noise. The slanted error bar at the lower right represents the correlated error in conductivity and density resulting from measurement of plasma radius from the streak photo. Theoretical curves are shown for Ebeling et al. [14] (——), Ichimaru and Tanaka [15] (- - -), Kurilenkov and Valuev [16] (- · - ·), and Lee and More [17] (· · ·).

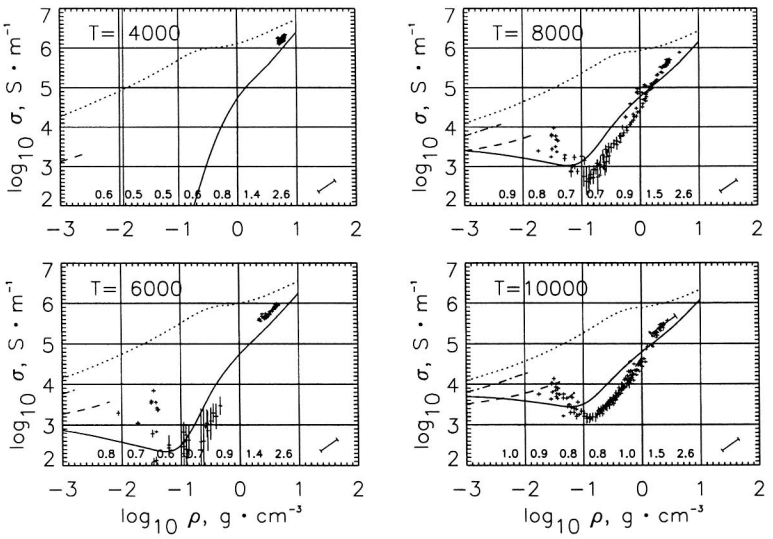

Fig. 6. Same as Fig. 5 for tungsten.

4. DISCUSSION

The trajectory profiles shown in Fig. 4 indicate that for the copper and aluminum shots the pressure rises sufficiently rapidly that the metal passes vertically out of the liquid–vapor coexistence region at nearly constant specific volume. In the case of tungsten, this occurs only on the highest-energy shots, and more typically the material only passes out of the coexistence region late in time. Figure 4c shows a case where the energy input just lifted the material to the vicinity of the critical point. No significant change in the electrical conductivity is noted in the data around the critical point in any of the three metals tested.

It is difficult to put an error estimate on these results, since the temperature depends on a theoretical equation of state that is given without error bars. The error in conductivity resulting from uncertainty in the column radius is shown in Figs. 5 and 6.

According to these measurements, the plasma conductivity is a strong function of the density and, at a high density, is almost-independent of temperature. As the density falls, the effect of temperature is more apparent. For the lower temperatures we see that the conductivity falls to a minimum at a few percent of solid density, then rises with further decrease in density,

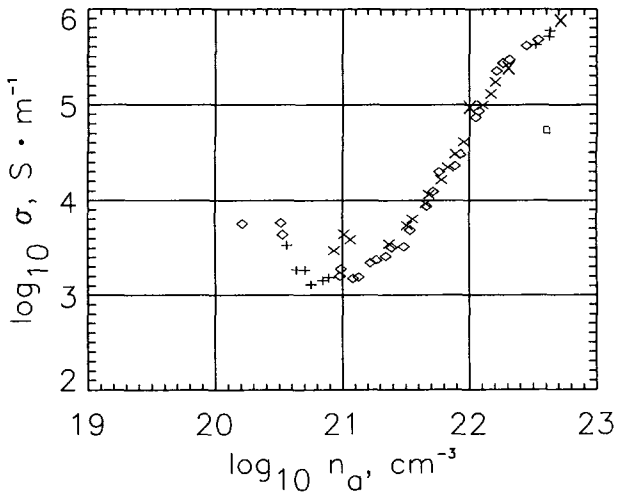

Fig. 7. Electrical conductivity of copper ($\diamond$), aluminum ($\times$), and tungsten (+) at $T = 10{,}000$ K, plotted as a function of atom density. The three large X's are representative data of Kloss et al. [12], and the square shows data from a slight extrapolation of the measurements of Mostovych and Chan [13].

eventually approaching the Spitzer conductivity [11] that is valid for tenuous plasmas.

If instead of plotting electrical conductivities versus mass density, we plot conductivity versus atom density, the curves become much more similar, shown in Fig. 7. It appears that the ion mass has little influence on the conductivity. In the tungsten case, we have compared our data with those of Kloss et al. [12], which show close agreement. We also show a point slightly extrapolated from the measurements by reflectivity of Mostovych and Chan [13].

Theoretical models for the electrical conductivity of strongly coupled plasmas have been given by a number of authors. We show in Figs. 5 and 6 the results of theory of Ebeling et al. [14], Ichimaru and Tanaka [15], Kurilenkov and Valuev [16], and Lee and More [17]. The best fits have been from a theory by Polischuk contained in the book by Ebeling et al. [14].

ACKNOWLEDGMENTS

This work was supported by the National Science Foundation. We thank David Gershon and Jeng-Mei Liu for their able assistance in the early stages of the work. The work would not have been possible without the expert technical help of our now-retired shop supervisor, Kenneth Diller.

REFERENCES

1. A. W. DeSilva and H.-J. Kunze, *Phys. Rev. E* **49**:4448 (1994).
2. A. W. DeSilva and J. D. Katsouros, *Phys. Rev. E* **57**:5945 (1998).
3. K. S. Fansler and D. D. Shear, in *Exploding Wires, Vol. 4*, W. G. Chace and H. K. Moore, eds. (Plenum, New York, 1959), pp. 185–193.
4. S. G. Barolskii, N. V. Ermokhin, P. P. Kulik, and V. A. Ryabyi, *High Temp.* **14**:626 (1976).
5. P. P. Kulik, E. K. Rozanov, and V. A. Ryabyi, *High Temp.* **15**:349 (1977).
6. V. M. Adamyan, G. A. Gulyi, N. L. Pushek, P. D. Starchik, I. M. Tkachenko, and I. S. Shvets, *High Temp.* **18**:186 (1980).
7. R. Shepherd, D. Kania, L. A. Jones, M. Maestas, D. Nothwing, and K. Stetler, *Bull. Am. Phys. Soc.* **32**:1818 (1987).
8. K. S. Trainor, *J. Appl. Phys.* **54**:2372 (1983).
9. M. N. Plooster, *Phys. Fluids* **13**:2665 (1970).
10. M. H. Rice and J. M. Walsh, *J. Chem. Phys.* **26**:824 (1957).
11. L. Spitzer, Jr., *Physics of Fully Ionized Plasmas* (Interscience, New York, 1956), p. 86.
12. A. Kloss, T. Motzke, R. Grossjohann, and H. Hess, *Phys. Rev. E* **54**:5851 (1996).
13. A. N. Mostovych and Y. Chan, *Phys. Rev. Lett.* **79**:5094 (1997).

14. W. Ebeling, A. Förster, V. E. Fortov, V. K. Gryaznov, and A. Ya. Polishchuk, *Thermophysical Properties of Hot Dense Plasmas* (B. G. Teubner Verlagsgesellschaft, Stuttgart, 1991), pp. 266–285.
15. S. Ichimaru and S. Tanaka, *Phys. Rev. A* **32**:1790 (1985).
16. Yu. K. Kurilenkov and A. A. Valuev, *Beitr. Plasmaphys.* **24**:161 (1984).
17. Y. T. Lee and R. M. More, *Phys. Fluids* **27**:1273 (1984).